Catalysis Today 147 (2009) 100–106

Contents lists available at ScienceDirect

Catalysis Today

journal homepage: www.elsevier.com/locate/cattod

Development of cobalt–copper nanoparticles as catalysts for higher alcohol synthesis from syngas

Nachal Devi Subramanian [a], G. Balaji [b], Challa S.S.R. Kumar [b], James J. Spivey [a,*]

[a] Cain Department of Chemical Engineering, Louisiana State University, Baton Rouge, LA 70802, USA
[b] Center for Advanced Microstructures & Devices, Louisiana State University, Baton Rouge, LA 70806, USA

ARTICLE INFO

Article history:
Available online 2 April 2009

Keywords:
Co
Cu
Core–shell nanoparticles
Syngas
CO hydrogenation
Higher alcohols

ABSTRACT

The synthesis of higher alcohols from syngas has been studied over different types of Cu-based catalysts. In order to provide control over the catalyst composition at the scale of a few nanometers, we have synthesized two sets of Co–Cu nanoparticles with novel structures by wet chemical methods, namely, (a) cobalt core–copper shell (Co@Cu) and (b) cobalt–copper mixed (synthesized by simultaneous reduction of metal precursors) nanoparticles. These catalysts were characterized by X-ray diffraction (XRD), transmission electron microscopy (TEM), X-ray photoelectron spectroscopy (XPS) and temperature programmed reduction (TPR). The catalysts were tested for CO hydrogenation at temperatures ranging from 230 °C to 300 °C, 20 bar and 18,000 scc/(hr.gcat). It was observed that the Co–Cu mixed nanoparticles with higher Cu concentration exhibit a greater selectivity towards ethanol and C_{2+} oxygenates. The highest ethanol selectivity achieved was 11.4% with corresponding methane selectivity of 17.2% at 270 °C and 20 bar.

1. Introduction

With today's increasing oil prices and declining fossil fuel resources, there is a need to look for alternative commercially viable energy sources. Bio-based fuel resources, particularly ethanol, have been studied extensively in the recent years as clean, sustainable and transportable fuel alternatives [1]. One promising process for bio-fuel production involves the conversion of bio-derived synthesis gas (syngas) to fuels and oxygenates. Syngas derived from biomass or coal is particularly interesting since both sources are abundant, and biomass is a renewable feedstock [2]. It is well known that syngas conversion to C_{2+} oxygenates is often limited by the formation of methane and methanol. However, C_{2+} alcohols are more desirable products, both as neat fuels [3–5], fuel additives or as a carrier for hydrogen to supply fuel cells. In addition to its potential application as a transportation fuel, ethanol has been considered as a feedstock for the synthesis of variety of chemicals, fuels and polymers [6,7]. It is estimated that ethanol could replace as much as one-third of the domestic petroleum use in the near future [8]. Hence, the development of a suitable and efficient catalyst to produce higher alcohols from syngas, coupled with an understanding of the underlying reaction mechanism, is clearly important.

The general mechanism of C_2 oxygenate formation from syngas has been extensively studied and the main steps are believed to be: (a) dissociative adsorption of CO and H_2, (b) formation of surface hydrocarbon $(CH_x)_{ads}$ and hydroxyl $(OH)_{ads}$ species and (c) CO insertion to form the C–C bond [9]. Ethanol formation is favored by a catalyst that selectively promotes the CO insertion reaction instead of the hydrogenation of the $(CH_x)_{ads}$ surface species, since hydrogenation of $(CH_x)_{ads}$ species leads to hydrocarbon formation [10].

The catalysts that have been studied for this reaction include Rh-based catalysts and alkali-promoted Cu-based catalysts [10]. Rh-based catalysts have been found, so far, to be the most selective catalysts for the synthesis of higher alcohols from CO hydrogenation [10]. The activity and selectivity of C_2^+ oxygenate synthesis on Rh catalysts has been attributed to their ability to catalyze both CO dissociation and CO insertion [11]. However, CO dissociation on surfaces such as fcc Rh(1 1 1) is almost impossible or very slow and the presence of steps/kinks are necessary to enhance the CO dissociation rate [12]. This is in agreement with the catalytic behavior of Rh in CO hydrogenation since it has been suggested that metals which adsorb CO strong enough to activate the molecule but do not dissociate it readily are active catalysts for the formation of oxygenates [13]. However, the high cost and limited availability of the precious Rh metal catalysts [14] have led to the

* Corresponding author. Tel.: +1 225 578 3690; fax: +1 225 578 1476.
E-mail address: jjspivey@lsu.edu (J.J. Spivey).

0920-5861/$ – see front matter © 2009 Elsevier B.V. All rights reserved.
doi:10.1016/j.cattod.2009.02.027

development of base metal catalysts such as modified Cu-based catalysts for this application. The advantage of having mixed metals (either alloy, core–shell or physical mixture) is that they can be used to prepare catalysts with different metal-promoter morphologies and to control atomic-level interactions. This may lead to further improvement in the selectivity to desired products.

The study of catalysis with nanoparticle surfaces is growing rapidly. Nanometer-sized metal/alloy particles are receiving great attention in modern chemical research because of their unique properties that are different from the corresponding bulk materials [15]. These unique properties affect the electronic, magnetic, optical and chemical properties which are applicable in such diverse fields as photochemistry, electrochemistry, optics, and catalysis [15]. The origin of their intriguing behavior is attributed to high surface-to-volume ratios which lead to large fractions of metal atoms available at the surface for catalysis [16].

Cobalt nanoparticles are expected to possess excellent magnetic, hardness and impact resistance properties. Recently cobalt nanoparticles have been used as catalysts as well [16]. Surfactants play a vital role in controlling the particle size and shape of nanoparticles synthesized using wet-chemical methods. De Silva et al. [17] have reported that the surfactants influence the reaction pathways, prior to nucleation, leading to the formation of cobalt nanoparticles. However, the surfactants required during the synthesis are retained on the surfaces and thus may also lead to loss of catalytic activity. Recently, bimetallic/core–shell nanoparticles are also receiving much attention since they offer high surface area coupled with the ability to provide multiple surfaces for catalysis providing added efficiency [18]. These nanostructured bimetallic materials are of economic interest as well since precious materials can be deposited on inexpensive cores [18].

Generally, a catalyst active for higher oxygenate synthesis must contain both adsorbed molecular CO, and surface carbon species produced by dissociative adsorption of CO. So the catalyst must be able to dissociate only a portion of the CO molecules and must balance this with the hydrogenation of the intermediate to form alcohols. Hydrogenation of the $(CH_x)_{ads}$ intermediate produces undesirable methane [10]. Keeping this in mind, we choose the combination of Co and Cu for this study due to the following reasons [19]:

(a) Co—dissociates CO and hydrogenates the resulting surface carbon species into hydrocarbons, e.g., in F-T synthesis [19].
(b) Cu—assists in non-dissociative activation of CO, e.g., in methanol synthesis [19].

Thus a combination of Co and Cu might be expected to adsorb molecular CO on the Cu, which can then react preferentially with the carbon chains generated on the Co, thereby leading to higher alcohols.

We are aware of no literature reports that use Co–Cu bimetallic nanoparticles as catalysts for CO hydrogenation reaction. Herein, we report the synthesis, characterization and catalytic activity of Co–Cu nanoparticles in the conversion of syngas to higher alcohols. A series of cobalt–copper nanoparticles were synthesized by wet chemical methods to achieve either core–shell nanoparticles or mixed nanoparticles and then tested for CO hydrogenation reaction in a fixed bed microreactor system. The focus of the present research is to investigate the Co–Cu nanoparticle catalysts for the synthesis of C_{2+} oxygenates from syngas via CO hydrogenation and the impact of reaction temperature on their activity and selectivity.

2. Experimental

All the catalyst syntheses were carried out under inert atmospheric conditions using commercially available reagents. Cobalt chloride, dodecyl-N,N-dimethy-3-ammonio-1-propanesulfonate (sulfobetaine SB-12, 98%), tetrahydrofuran (THF), sodium borohydride, 1 M lithium hydrotriethylborate in THF, copper sulfate and sodium citrate hexahydrate were purchased from Aldrich Chemical Company and were used without further purification. Commercial cobalt nanoparticles, dispersed in toluene, were purchased from Strem chemicals. All the solvents used were degassed prior to use.

2.1. Synthesis of Co@Cu core–shell nanoparticles

2.1.1. Synthesis of cobalt (core) nanoparticles

Two sets of Co core nanoparticles were used—Co nanoparticles that were (1) commercially purchased from Strem chemicals (dispersed in toluene) and (2) chemically synthesized using water as the solvent and SB-12 as surfactant [18]. A mixture of cobalt chloride and SB-12 was placed in a three-necked flask which was evacuated and then filled with nitrogen three times. Degassed water was added to the flask under sonication and the contents were dissolved. Sodium borohydride was dissolved in water separately and this solution was added drop wise into the earlier $CoCl_2$ mixture over a period of 30 min. The pale pink solution turned black immediately upon addition, indicating the formation of cobalt nanoparticles. After the addition is complete, the reactants were stirred for an additional hour to ensure completion of the reaction, followed by the addition of 15 ml of acetone to destroy the excess reducing agent. The resulting cobalt nanoparticles were separated, washed thoroughly with degassed water followed by ethanol, and dried to obtain a fine powder.

2.1.2. Displacement formation of copper shell

The procedure as described by Guo et al. [18] was used to develop a shell around the two sets of cobalt nanoparticles. In a typical process, cobalt nanoparticles were added to a copper–citrate electrolyte, containing 0.25 M $CuSO_4{\cdot}5H_2O$ and 0.3 M $C_6H_5Na_3O_7{\cdot}2H_2O$ at a pH of 4.0. The reactants were sonicated for an hour under nitrogen environment. Fig. 1 illustrates this synthesis procedure. The particles were then separated using a magnet and washed thoroughly with degassed water followed by ethanol, then dried to obtain a fine powder. The final core–shell catalyst obtained from the commercial cobalt nanoparticles is designated as Co@Cu-1 and the one from water dispersible cobalt nanoparticles, synthesized in our lab using water as solvent, is designated as Co@Cu-2 in this paper.

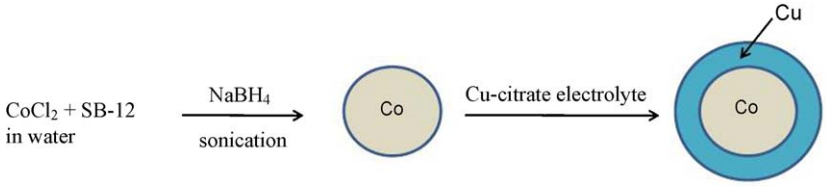

Fig. 1. Illustration of the synthesis of Co core @ Cu shell nanoparticles.

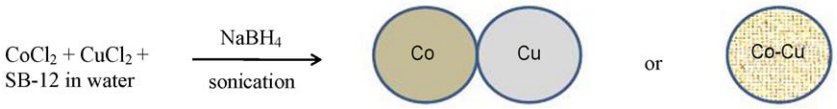

Fig. 2. Illustration of the synthesis of Co–Cu mixed nanoparticles.

2.2. Synthesis of Co–Cu mixed nanoparticles

Co–Cu mixed nanoparticles were synthesized in the same way as the cobalt core nanoparticles, except that the chloride salts of cobalt and copper were reduced simultaneously in the presence of SB-12 surfactant in water using $NaBH_4$ as a reducing agent under sonication. Fig. 2 illustrates the method by which these mixed nanoparticles were synthesized. This synthesis may lead to two possible forms of these Co–Cu mixed nanoparticles: a mixture of copper and cobalt, or Co–Cu alloy nanoparticles. Two catalysts with different initial molar ratios of Co and Cu (1:5 and 1:10 by mole) were synthesized by this method. These catalysts are, henceforth, designated as Co–Cu(1:3) and Co–Cu(1:24) respectively (the ratios in parentheses indicate the final atomic ratios of Co and Cu as obtained by ICP results, discussed later).

2.3. Characterization

The Co–Cu core–shell and mixed nanoparticles were characterized by transmission electron microscopy (TEM), X-ray diffraction (XRD), X-ray photoelectron spectroscopy (XPS), inductively coupled plasma atomic emission spectrometry (ICP) and temperature programmed reduction (TPR). Size and size-distribution of the nanoparticles were analyzed using TEM experiments carried out using Hitachi H-7600 with a 125 kV accelerating voltage and operated on a JEOL 100CX at 80 kV. Samples for TEM were prepared in inert atmospheric conditions by adding ethanol to the Co–Cu nanoparticles, ultrasonicating them for a few seconds and then placing them on carbon-coated gold grids. X-ray diffraction (XRD) patterns were recorded on a Bruker/Siemens D5000 automated powder X-ray diffractometer, using Cu Kα radiation (λ = 1.540562 Å) with Rietveld analysis software. XPS studies were performed on a Kratos AXIS 165 X-ray Photoelectron Spectroscope and Scanning Auger Microscope equipped with standard Mg/Al source and high performance Al monochromatic source. Inductively coupled plasma (ICP) atomic emission spectrometry was used for the determination of the bulk metal content in each sample. The ICP measurements were performed with a Spectro Ciros Inductively Coupled Plasma Analyzer in the Central Analytical Instruments Research Laboratory, LSU Ag Center, LSU.

TPR experiments were carried out in a fixed bed microreactor system. 200 mg of the sample was placed in a 1/4 in. reactor tube and reduced in a 10% H_2/Ar mixture while the temperature was linearly ramped from room temperature to 500 °C at 5 °C/min. A thermal conductivity detector (TCD) was used to follow H_2 consumption as a function of temperature. Sample preparation for all the techniques was carried out in atmospheric conditions except for TEM.

2.4. CO hydrogenation reaction

CO hydrogenation reactions, using the synthesized catalysts, were performed in a fixed bed microreactor system at differential conversions. The catalyst (0.2 g) was loaded between quartz wool and placed in the middle of the reactor with a thermocouple close to the catalyst packing. Prior to reaction, the catalyst was reduced at 300 °C in flowing 75% H_2/He for 2 h at atmospheric pressure. The reaction then started as gas flow was switched to H_2/CO mixture (molar ratio of H_2/CO = 2) at the reaction temperature and pressure. The products were analyzed for both oxygenates and hydrocarbons in an Agilent GC 6890 with MSD and TCD.

All the four catalysts, namely, Co@Cu-1, Co@Cu-2, Co–Cu(1:3) and Co–Cu(1:24), were tested at three different temperatures at a pressure of 20 bar, H_2/CO ratio of 2:1 and space velocity (SV) of 18,000 scc/(hr.gcat) . Product selectivities are reported in terms of carbon efficiencies which is defined as

$$\text{Carbon efficiency} = \frac{n_i C_i}{\Sigma(n_i C_i)}$$

where n_i is the number of carbon atoms and C_i is the molar concentration of the carbon-containing products.

3. Results and discussion

3.1. TEM

Fig. 3(a)–(d) shows the TEM bright-field micrographs of Co@Cu-1, Co@Cu-2, Co–Cu(1:3) and Co–Cu(1:24) nanoparticles respectively. The morphology of all the particles irrespective of the synthetic conditions is spherical in nature, while the mean diameters of the particles vary. TEM shows a slight aggregation of the particles, but they are still fairly uniform and the mean diameters are roughly around 9 nm, 7.5 nm, 12 nm and 25 nm respectively for Co@Cu-1, Co@Cu-2, Co–Cu(1:3) and Co–Cu(1:24) systems.

In both the samples synthesized by core–shell method, the expected core–shell structure is not clearly distinguishable from the TEM images and this may be due to very small difference in atomic numbers between Co and Cu [18].

3.2. XRD

Fig. 4 shows the XRD patterns for the two sets of Co–Cu nanoparticles. The peaks can be identified as face-centered cubic Cu as indicated in the figure. As can be seen, for all the catalysts, a single pattern corresponding to Cu is prominent, probably indicating either the higher dispersion or the amorphous nature of cobalt. XRD peaks are observed at d = 2.09, 1.81 and 1.28 Å, which are in a good agreement with the standard XRD pattern, ICDD (040836) of metallic Cu. However, a small peak at around $2\theta = 36.2°$ and d = 2.48 Å for the case of Co–Cu(1:24) catalyst (Fig. 2(d)) indicates the presence of minor amounts of Cu_2O based on ICDD (030892). No clear or distinct peak was detected for Co, consistent with the results of others [20], which may also imply the formation of solution in the immiscible Co–Cu systems. For the case of Co–Cu mixed nanoparticles, there is no evidence for the formation of an alloy. This suggests that a mixture of cobalt and copper nanoparticles was formed in our experiment. The absence of Co peaks may also be due to the fact that Cu Kα radiation source was used in the XRD measurements. Utilization of Co Kα radiation source might have provided better resolution in the diffraction patterns of cobalt as often Cu Kα radiation results in higher fluorescence and therefore more background noise in XRD spectra of cobalt nanoparticles [21].

3.3. XPS

XPS studies of the as-prepared samples were carried out in order to study the chemical state of the elements at the catalytic surface. Typical spectra of the samples for the Co ($2p_{3/2}$) and Cu

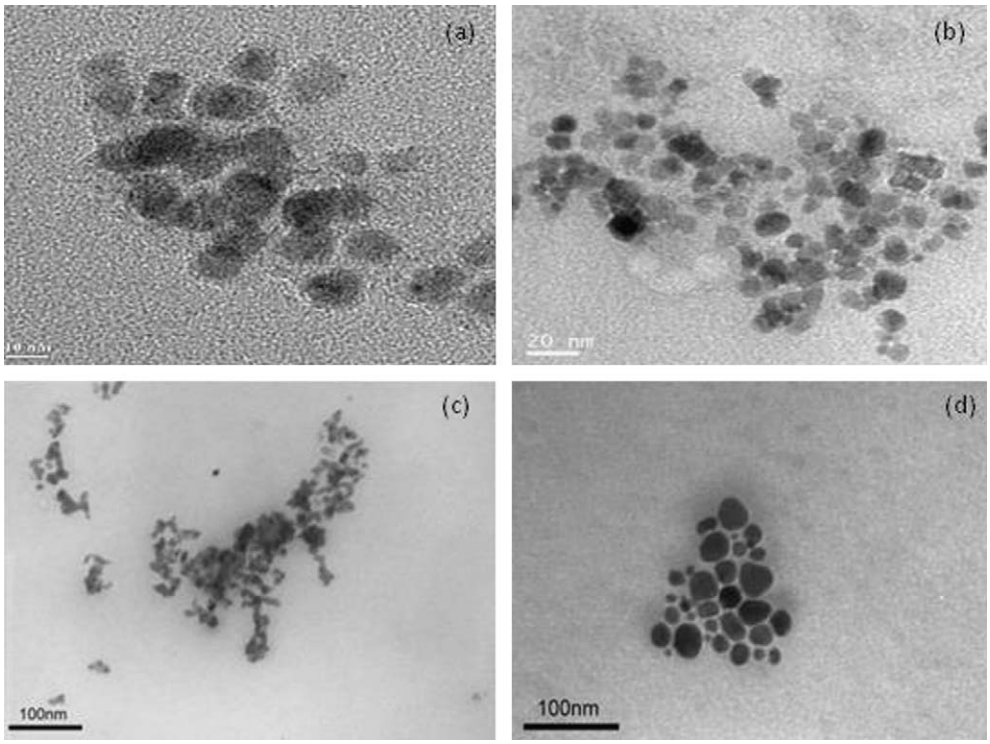

Fig. 3. TEM images of (a) Co@Cu-1 (b) Co@Cu-2 (c) Co–Cu(1:3) and (d) Co–Cu(1:24) nanoparticle catalysts.

($2p_{3/2}$) regions are shown in Figs. 5 and 6 respectively, and Table 1 gives the data in terms of binding energies of the main cobalt and copper peaks. Table 1 also summarizes the bulk (obtained from ICP results) as well as Cu/Co surface atomic ratios of the nanoparticle catalysts.

The Cu $2p_{3/2}$ and the Co $2p_{3/2}$ transitions are characterized by a main peak with a satellite on the higher binding energy side for both copper and cobalt in bivalent chemical state [22,23]. For the Co@Cu-1 catalyst, the Cu $2p_{3/2}$ main peak is centered at 930.6 eV whilst the Co 2p3/2 main peak is positioned at 779.3 eV; for copper, the binding energy and the presence of the satellite peak suggest that it is present as the divalent ion (Cu^{2+}) and cobalt ions remain in the form of Co_3O_4 (no shake-up satellites) [19]. In the case of Co@Cu-2 catalyst, both cobalt and copper are present in +2 oxidation states as indicated by the peaks at 781 eV and 933.2 eV respectively [22,23].

For the Co–Cu(1:3) catalyst, the Cu $2p_{3/2}$ main peak is centered at 932.2 eV and from the shape of the spectrum (i.e. the weakness of satellite structure), the existence of Cu^{+} or Cu^{0} metallic species can be postulated [23,24]. The Co $2p_{3/2}$ main peak is positioned at 780.1 eV which corresponds to both Co^{2+} and Co^{3+} ions. These values are consistent with the data reported by Chuang et al. [25].

In the case of Co–Cu(1:24) sample, the Cu $2p_{3/2}$ peak at 931.9 eV suggests that copper is present in +1 oxidation state. The binding energy of the Co $2p_{3/2}$ peak increased to 782.3 eV with the shake-up satellite appearing at higher binding energy. This value seems higher

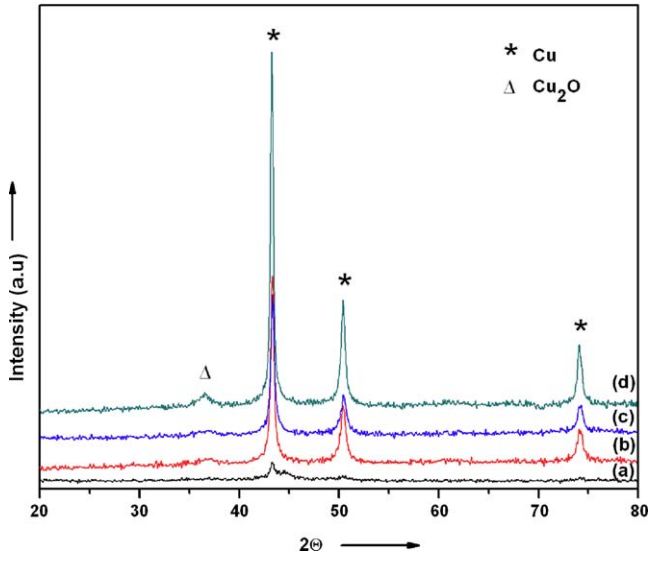

Fig. 4. Powder X-ray diffraction patterns of (a) Co@Cu-1 (b) Co@Cu-2 (c) Co–Cu(1:3) and (d) Co–Cu(1:24) nanoparticle catalysts.

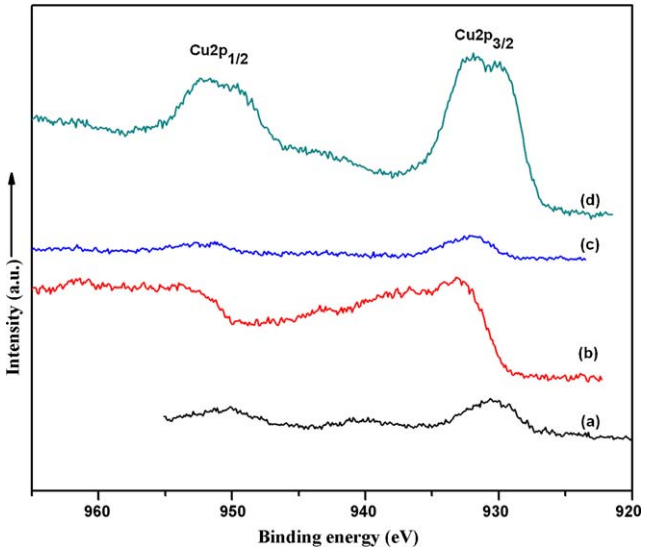

Fig. 5. XPS spectrum of the Cu 2p region for (a) Co@Cu-1 (b) Co@Cu-2 (c) Co–Cu(1:3) and (d) Co–Cu(1:24) nanoparticle catalysts.

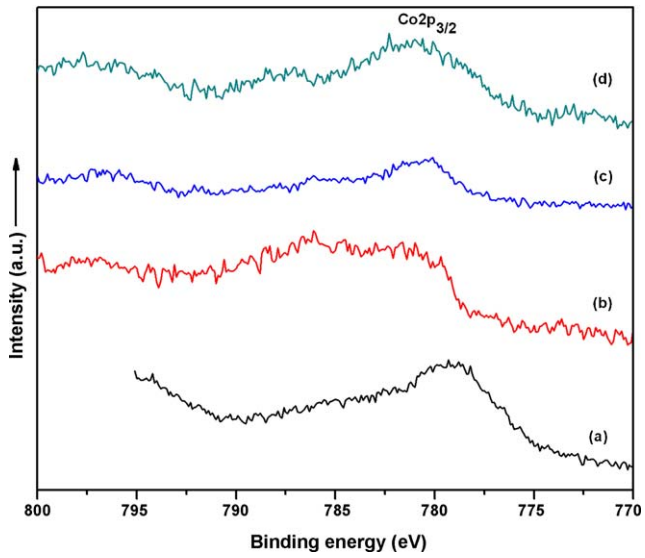

Fig. 6. XPS spectrum of the Co 2p region for (a) Co@Cu-1 (b) Co@Cu-2 (c) Co–Cu(1:3) and (d) Co–Cu(1:24) nanoparticle catalysts.

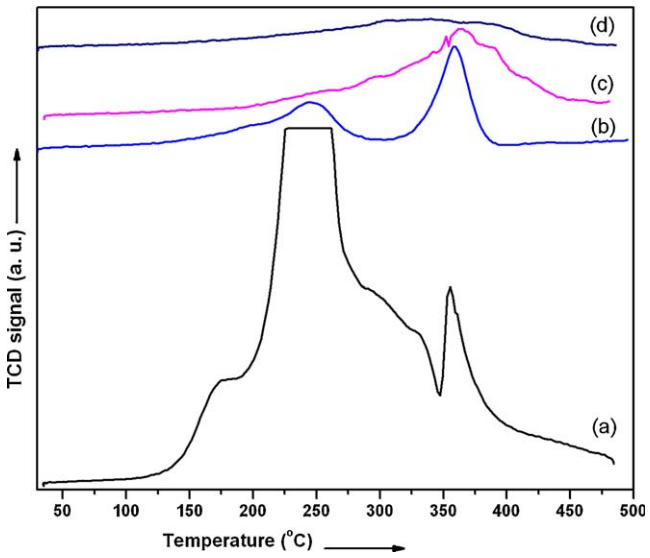

Fig. 7. TPR of the Co–Cu nanoparticle catalysts (a) Co@Cu-1 (b) Co@Cu-2 (c) Co–Cu(1:3) and (d) Co–Cu(1:24).

Table 1
XPS & ICP analysis of Co–Cu nanoparticle catalysts.

Catalyst	Binding energies (eV)		Cu/Co atomic ratio by XPS	Cu/Co atomic ratio by ICP
	Cu $2p_{3/2}$	Co $2p_{3/2}$		
Co@Cu-1	930.6	779.3	0.9	0.5
Co@Cu-2	933.2	781	2.1	7.3
Co–Cu(1:3)	932.2	780.1	1.1	3.1
Co–Cu(1:24)	931.9	782.3	2.4	24.9

compared to a spectrum characteristic of Co^{2+} (781 ± 0.5 eV) in the form of CoO. But as reported in literature, cobalt may be present as the divalent ion [19]. Further evidence for this is given by the fact that the difference in binding energy between Co ($2p_{3/2}$) and Co ($2p_{1/2}$) is 15.4 eV which is in agreement with the literature [26]. The surface oxidation in all the catalysts may be due to the exposure to air during sample preparation. The nanoparticles, especially the metallic cobalt nanoparticles, are extremely sensitive to atmospheric oxygen [18] and a thin layer of cobalt oxide is readily formed [21] which could be a major reason for the oxidation signatures in XPS measurements. However, the catalysts are reduced at 300 °C prior to the CO hydrogenation reaction.

3.4. TPR

Fig. 7 shows the TPR profiles of the four Co–Cu nanoparticle catalysts. The TPR profiles of both the core–shell catalysts, Co@Cu-1 and Co@Cu-2 (Fig. 7(a) and (b)), are similar, characterized by two prominent peaks centered at 250 °C and 355 °C. The lower temperature peak at 250 °C with a small shoulder can be attributed to the sequential reduction of Cu^{2+} to Cu^0 ions whereas the second peak at 355 °C with a small shoulder on the right can be attributed to the reduction of Co^{3+} ions [27]. The TPR for Co@Cu-1 is qualitatively similar to Co@Cu-2, with peaks at 250 °C and 355 °C, but far more H_2 is consumed which suggests that this catalyst may have been more susceptible to atmospheric oxidation.

For the case of mixed nanoparticles, Co–Cu(1:3) and Co–Cu(1:24), the TPR profiles are characterized by a single peak centered at ~360 °C, which can be once again attributed to the reduction of Co^{3+} ions. But there is no separate peak at lower temperatures for the reduction of copper. This might suggest that copper in these catalysts is less sensitive to atmospheric oxidation and so it remains in metallic state. Comparison between all four catalysts (Fig. 7(a)–(d)) reveals that the relative intensities of the peaks are dependent on the Cu/Co atomic ratio since both the higher and lower temperature peaks decrease in size with decreasing the cobalt content.

3.5. CO hydrogenation results

The influence of the reaction temperature on the product selectivities has been examined in the range of 230–300 °C under 20 bar and $H_2/CO = 2$ over the four catalysts investigated here. Fig. 8 shows the result of a thermodynamic analysis of the CO hydrogenation reaction for a wide range of products (methane, CO_2, H_2O, ethanol and C_{2+} oxygenates) as a function of temperature, assuming a stoichiometric mixture of CO and H_2 ($H_2/CO = 2.0$) at 20 bar. Ethanol selectivity at equilibrium is virtually zero at all temperatures when methane is allowed as a product which is also reported by Spivey and Egbebi [10]. Thus, to increase the ethanol yield and selectivity, the thermodynamically favored methane formation must be kinetically limited.

Table 2 summarizes the effects of temperature on product selectivities of the four Co–Cu catalysts. It is evident that the reaction temperature has a profound effect on the selectivity of the

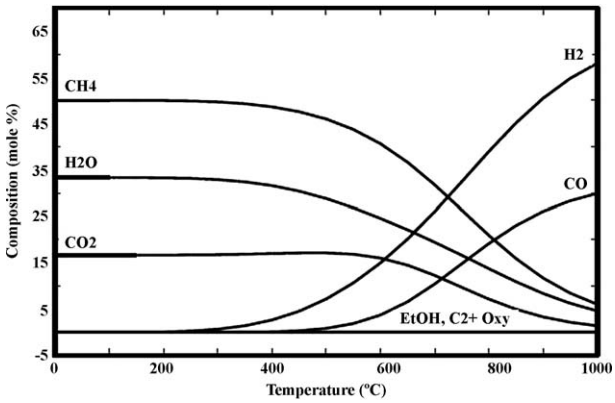

Fig. 8. Equilibrium composition for the hydrogenation of CO to ethanol, with methane and C_{2+} oxygenates formation allowed ($H_2/CO = 2$, 20 bar, calculated using HSC software).

Table 2
Effect of temperature on the product selectivities of Co–Cu nanoparticle catalysts.

(a) Product selectivities of Co–Cu nanoparticle catalysts at 230 °C[a]

Catalyst	Selectivity (% C)[b]					
	CO_2	CH_4	MeOH	EtOH	C_{2+} Oxy[c]	C_{2+} HC[d]
Co@Cu-1	9.5	59.1	0.9	0.6	5.0	25.2
Co@Cu-2	30.3	31.6	3.4	5.4	24.2	5.1
Co–Cu(1:3)	14.3	60.6	1.2	2.4	16.0	5.5
Co–Cu(1:24)	39.8	16.7	5.6	9.6	28.3	0.03

(b) Product selectivities of Co–Cu nanoparticle catalysts at 270 °C[a]

Catalyst	Selectivity (% C)[b]					
	CO_2	CH_4	MeOH	EtOH	C_{2+} Oxy[c]	C_{2+} HC[d]
Co@Cu-1	16.6	40.2	1.3	2.1	2.6	37.4
Co@Cu-2	19.1	47.1	2.5	2.7	3.7	24.9
Co–Cu(1:3)	27.8	28.9	2.8	5.3	35.2	0.2
Co–Cu(1:24)	48.8	17.2	6.6	11.4	16.0	0.1

(c) Product selectivities of Co–Cu nanoparticle catalysts at 300 °C[a]

Catalyst	Selectivity (% C)[b]					
	CO_2	CH_4	MeOH	EtOH	C_{2+} Oxy[c]	C_{2+} HC[d]
Co@Cu-1	41.6	30.5	0.3	0.7	1.4	25.6
Co@Cu-2	13.7	45.4	1.5	1.7	1.7	36.2
Co–Cu(1:3)	26.4	39.0	2.6	5.0	23.9	3.2
Co–Cu(1:24)	30.7	15.6	3.5	6.0	41.5	2.7

[a] Catalyst: 0.2 g; reaction conditions: P = 20 bar, $H_2/CO = 2$, space velocity = 18,000 scc/(hr.gcat).
[b] Product selectivities are reported in terms of carbon efficiencies defined as Carbon efficiency = $n_iC_i/\Sigma(n_iC_i)$ where n_i is the number of carbon atoms and C_i is the concentration of the carbon-containing products.
[c] Oxygenates with 2 or more carbons except ethanol (acetaldehyde, acetone, i-propanol, i-butanol, n-propanol and n-butanol).
[d] Hydrocarbons with 2 or more carbons (ethane, propane, i-butane, n-butane, n-hexane and propylene).

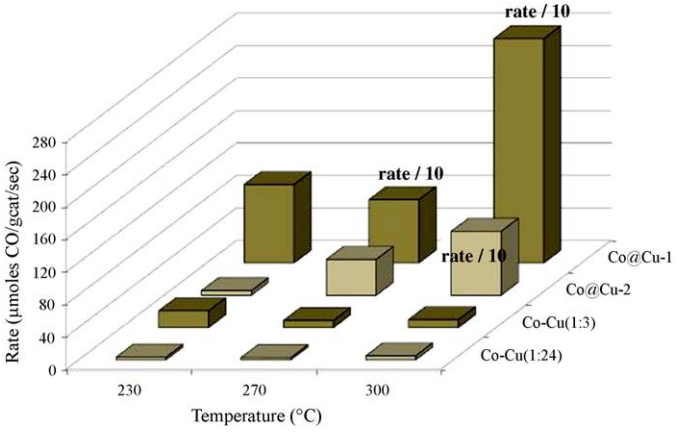

Fig. 9. CO conversion rate as a function of temperature ($H_2/CO = 2$, 20 bar, 18,000 scc/(hr.gcat).

catalyst. Oxygenates and hydrocarbons are always accompanied by the production of water, most of which appears to be converted to CO_2 through the water–gas-shift reaction [27]. Tables 2a and 2b demonstrate that increasing the temperature from 230 °C to 270 °C results in a notable increase in ethanol, methanol and CO_2 selectivities and a considerable decrease in methane selectivity in some catalysts. However, further increasing the temperature to 300 °C favors higher hydrocarbons (Table 2c).

Clearly, the mixed Co–Cu(1:24) nanoparticles have higher ethanol selectivity at the temperatures tested. The trend in ethanol and C_{2+} oxygenate selectivities at 230 °C can be correlated to Cu/Co atomic ratios obtained from XPS and ICP results (see Table 1). That is, Co–Cu(1:24) which has the highest Cu/Co atomic ratio leads to higher ethanol and C_{2+} oxygenates followed by Co@Cu-2 and then the other two catalysts which have lower Cu/Co atomic ratios.

But this trend is not observed at 270 °C and 300 °C. From the results presented in Tables 2a–2c, it is evident that in the case of Co–Cu mixed nanoparticle systems, the selectivity to ethanol, methanol and CO_2 go through a maximum as a function of temperature. This behavior may be associated with the sintering of the nanoparticles at higher temperatures which leads to a higher selectivity towards hydrocarbons [28]. Another possible explanation would be associated with the higher activation energy for hydrogenation of the carbonaceous intermediate than for CO insertion, which is supported by the increased hydrocarbon production with increasing temperature [29]. The high selectivity towards CO_2 formation can be attributed to the presence of surface copper (Table 1) that enhances the water gas shift reaction. Comparison between the two Co–Cu mixed nanoparticle catalysts shows a higher selectivity towards ethanol with increasing Cu/Co atomic ratio, that is, Co–Cu(1:24) is more selective than the Co–Cu(1:3) catalyst.

In the case of core–shell catalysts, Co@Cu-1 follows a similar trend as that for the mixed nanoparticles except that majority of the products consist of hydrocarbons. However, on the Co@Cu-2 catalyst, ethanol selectivity decreases and methane selectivity increases with temperature. There is a considerable increase in the total hydrocarbon selectivity with temperature for the core–shell catalysts (Co@Cu-1 and Co@Cu-2) and this may be attributed to lower Cu/Co atomic ratios on the surface which result in increased conversion of CO into hydrocarbons. Consequently, the total selectivity to alcohols gradually decreased and hydrocarbon selectivity increased over these samples. These observations are consistent with those of Courty et al. [30] and De Aquino et al. [31], who observed high methane selectivity over Cu–Co–Al catalysts.

Metallic cobalt is active in the dissociative adsorption of CO, C–C chain growth and hydrocarbon production [29]. Nonetheless, suppression of hydrocarbon formation was seen on the mixed nanoparticle samples at 270 °C, perhaps due to enhanced stability of the CH_x species on the surface, followed by CO insertion into the M–C bond of the surface CH_x species and hydrogenation to produce alcohols [29,32]. The termination and alcohol production step can be attributed to the role of copper which assists in non-dissociative activation of CO [19]. Among all the four catalysts, the Co–Cu(1:24) catalyst showed the highest selectivity towards ethanol with the maximum at 270 °C (11.4%) with reduced methane selectivity (17.2%).

Fig. 9 depicts the variations in the rates of CO conversion (reported in μmoles/gcat/s) as a function of temperature for all four catalysts. Increasing the reaction temperature to 300 °C increased the CO conversion rate rapidly for the case of core–shell catalysts, whereas, it goes through a minimum at 270 °C for the mixed nanoparticle catalysts. Hence, we find that the Co–Cu mixed nanoparticle catalysts are much less active than the core–shell catalysts, but are more selective towards ethanol formation. This might be because hydrocarbon formation, which typically accompanies high catalytic activity, is suppressed on these catalysts.

4. Conclusions

A series of Co–Cu core–shell and mixed nanoparticle catalysts were synthesized and tested for CO hydrogenation. It was found that the mixed nanoparticle catalysts are more selective to ethanol and higher oxygenates than the core–shell catalysts whereas the latter are more active but not selective to ethanol. The mixed nanoparticle catalysts are not active because hydrocarbon formation, which typically accompanies high catalytic activity, is suppressed. Thus, further modifications in the design of our Co–Cu catalysts are necessary in order to balance between the catalyst

activity and selectivity to obtain a high yield of ethanol. Also the Co–Cu composition has to be chosen in such a way that there is a proper balance between CO dissociation and CO insertion that is necessary for the synthesis of higher alcohols. The present investigation also indicates that the CO conversion and product selectivity of the Co–Cu bimetallic catalysts is strongly influenced by reaction temperature. Under the reaction conditions of this study, the highest ethanol selectivity achieved was 11.4% for Co–Cu(1:24) catalyst with 17.2% methane selectivity.

Investigations are continuing in order to optimize the Co–Cu nanoparticle catalysts, to understand the reaction mechanisms, and to develop the next generation of catalysts with higher ethanol yield. Detailed study will also be carried out on the Co–Cu bimetallic nanoparticle synthesis to obtain selectively alloy, core–shell and mixed metal catalysts. Further studies to investigate the effect of pressure, H_2/CO ratio, space velocity and alkali promoters are currently under progress.

Acknowledgements

The authors thank the U.S. Department of Energy and the project officer Dr. Dan Driscoll for providing financial support, under the Contract DE-FC26-06NT43024. Nachal Subramanian also thanks LSU-CAMD for partial fellowship support. CSSRK gratefully acknowledges funding from National Academies Keck Futures Initiative (NAKFI) to prepare nanostructured Co–Cu materials.

References

[1] X. Pan, Z. Fan, W. Chen, Y. Ding, H. Luo, X. Bao, Nature Mater. 6 (2007) 507.
[2] A.M. Henstra, J. Sipma, A. Rinzema, A.J.M. Stams, Curr. Opin. Biotechnol. 18 (2007) 200.
[3] S. Velu, N. Satoh, C.S. Gopinath, K. Suzuki, Catal. Lett. 82 (2002) 145.
[4] D.A. Deluga, J.R. Salge, L.D. Schmidt, X.E. Verykios, Science 303 (2004) 993.
[5] S. Velu, C. Song, in: J.J. Spivey (Ed.), Catalysis, vol. 20, Royal Society of Chemistry, London, 2007, 65 pp.
[6] B.O. Palsson, S. Faith-Afshar, D.F. Rudd, E.N. Lightfoot, Science 213 (1981) 513.
[7] T.K. Ng, R.M. Busche, C.C. Mcdonald, R.W.F. Hardy, Science 219 (1983) 4585.
[8] J.D. Mackaluso, MMG 445 Basic Biotechnology eJournal 3 (2007) 98.
[9] P. Gronchi, E. Tempesti, C. Mazzocchia, Appl. Catal. A: Gen. 120 (1994) 115.
[10] J.J. Spivey, A. Egbebi, Chem. Soc. Rev. 36 (2007) 1.
[11] S.S.C. Chuang, R.W. Stevens, R. Khatri, Top. Catal. 32 (2005).
[12] V.V. Gorodetskii, B. Nieuwenhuys, Surf. Sci. 105 (1981) 299.
[13] M.L. Poutsma, L.F. Elek, P.A. Iborbia, A.P. Risch, J.A. Rabo, J. Catal. 52 (1978) 157.
[14] V. Subramani, K. Gangwal, Energy Fuels 22 (2) (2008) 814.
[15] Y. Song, E.E. Doomes, J. Prindle, R. Tittsworth, J. Hormes, C.S.S.R. Kumar, J. Phys. Chem. B 109 (2005) 9330.
[16] M. Salavati-Niasari, F. Davar, M. Mazaheri, M. Shaterian, J. Magn. Magn. Mater. 320 (2008) 575.
[17] R.M. De Silva, V. Palshin, K.M.N. De Silva, L.L. Henry, C.S.S.R. Kumar, J. Mater. Chem. 18 (2008) 738.
[18] Z. Guo, C.S.S.R. Kumar, L.L. Henry, E.E. Doomes, J. Hormes, E.J. Podlaha, J. Electrochem. Soc. 152 (1) (2005) D1–D5.
[19] N. Mouaddib, V. Perrichon, G.A. Martin, Appl. Catal. A: Gen. 118 (1994) 63.
[20] Z.Q. Yang, C.Y. You, L.L. He, J. Alloys Compd. 423 (2006) 128.
[21] Song, et al. Chem. Mater. 18 (12) (2006) 2817.
[22] A. Cimino, B.A. De Angelis, G. Minelli, Surf. Interface Anal. 5 (1983) 150.
[23] D.C. Frost, A. Ishitani, C.A. McDowell, Mol. Phys. 24 (1972) 861.
[24] S. Larsson, Chem. Phys. Len. 40 (3) (1976) 362.
[25] T.J. Chuang, C.R. Brundle, D.W. Rice, Surf. Sci. 59 (3) (1976) 41.
[26] K. Sato, Y. Inoue, I. Kojima, B. Miyazaki, I. Yasumoti, J. Chem. Soc. Faraday Trans. 180 (1984) 841.
[27] N. Tien-Thao, M.H. Zahedi-Niaki, H. Alamdari, S. Kaliaguine, Appl. Catal. A: Gen. 326 (2007) 152.
[28] P. Chaumette, P. Courty, et al. Ind. Eng. Chem. Res. 33 (1994) 1460.
[29] J.A. Dalmon, P. Chaumette, C. Mirodatos, Catal. Today 15 (1992) 101.
[30] P. Courty, D. Durand, E. Freund, A. Sugier, J. Mol. Catal. 17 (1982) 241.
[31] A.D. De Aquino, A.J.G. Cobo, Catal. Today 65 (2001) 209.
[32] P. Chaumette, P. Courty, A. Kiennemann, B. Ernst, Top. Catal. 2 (1995) 117.